Ductile rupture under cyclic loadings at high triaxiality: The influence of strain hardening and elasticity

Almahdi Remmal, Jean-Baptiste Leblond

Ductile rupture under cyclic loadings at high triaxiality: the influence of strain hardening and elasticity

Almahdi Remmal[1], Jean-Baptiste Leblond[2,3] *

[1] *FRAMATOME, Tour Framatome, 1 place Jean Millier, 92084 Paris La Défense Cedex, France*

[2] *Sorbonne Université, CNRS, UMR 7190, Institut Jean Le Rond d'Alembert, Tour 65-55, 4 place Jussieu, 75232 Paris Cedex 05, France*

[3] *ESI-Group, Immeuble Le Récamier, 70 rue Robert, 69458 Lyon Cedex 06, France*

Abstract

Previous works (Devaux *et al.*, 1997; Cheng *et al.*, 2017) have emphasized the effects of strain hardening and elasticity upon ductile rupture of metals under cyclic loading conditions. This work pursues the study and modelling of these two effects by distinct theoretical methods, each coupled with micromechanical finite element simulations of the behaviour of some "representative cell". For the effect of strain hardening, we employ Morin *et al.* (2017)'s approach, based on the theory of *sequential limit-analysis* (Yang, 1993; Leu, 2007; Leblond *et al.*, 2018). This approach is applied to various types of hardening of the metallic matrix: isotropic, linear kinematic, nonlinear kinematic with one or two kinematic variables (Armstrong and Frederick, 2007), and even a simplified version of Chaboche (1991)'s model accounting for complex cyclic effects. Numerical micromechanical simulations of a hollow sphere made of elastic-plastic materials obeying the various hardening laws considered, and subjected to cyclic loadings at high triaxiality, fully confirm the predictions of the model developed, provided elasticity is made negligible by using an artificially high value of Young's modulus. When a realistic value is employed, however, the agreement between theoretical predictions and numerical results is degraded, thus emphasizing again the importance of the effect of elasticity in cyclic ductile rupture. To deal with this effect we derive, apparently for the first time, an evolution equation of the porosity accounting for (compressible) elasticity. However, numerical micromechanical simulations reveal that simply using this new evolution law, while keeping all other aspects of the model unchanged, remains insufficient to get a good match of theoretical and numerical results. Such a match is achieved by introducing the *ad hoc* hypothesis that the yield criterion and flow rule derived from sequential analysis still apply in the presence of elasticity, but with some "effective porosity" slightly differing from the true one through some heuristic, adjustable factor.

Key words: Porous ductile materials, cyclic loadings, strain hardening, elasticity

* Corresponding author.

1 Introduction

It is a well established experimental fact that the ductility (strain to fracture) of ductile metals and alloys is notably lower under cyclic loadings than under monotonic ones (Schmidt *et al.*, 1991; Kobayashi *et al.*, 1992). The study and modelling of this phenomenon are obviously of major importance for the prediction of the risks of ductile rupture in metallic structures subjected to cyclic loading conditions. On the basis of micromechanical finite element simulations of the behaviour of hollow plastic cells loaded cyclically, Gilles *et al.* (1992) tentatively ascribed the effect to some *ratcheting of the porosity* under such conditions (gradual increase, with the number of cycles, of the maximum porosity reached during each one). This interpretation was duly confirmed by Devaux *et al.* (1997), through more accurate numerical simulations. Many works on the topic, mostly based again on micromechanical simulations, followed (Besson and Guillemer-Neel, 2003; Brocks and Steglich, 2003; Rabold and Kuna, 2005; Steglich *et al.*, 2005; Mbiakop *et al.*, 2015; Lacroix *et al.*, 2016; Cheng *et al.*, 2017; Nielsen *et al.*, 2018).

With regard to theoretical aspects, two fundamental remarks were made by Devaux *et al.* (1997) and elaborated by Lacroix *et al.* (2016):

(1) The ratcheting of the porosity, and more generally the asymmetry of successive half-cycles in tension and compression, basically arises from two distinct aspects of the mechanical behaviour: *strain hardening* and/or *elasticity*. In other words, for *rigid-ideal-plastic* materials devoid of both elasticity and hardening, successive half-cycles are perfectly symmetrical, and the evolution of the porosity during one cycle instantly stabilized. [1]

(2) Gurson (1977)'s classical model for the overall behaviour of porous plastic materials fails - even in its extended form known as the GTN model (Tvergaard, 1981; Tvergaard and Needleman, 1984) - to predict any ratcheting of the porosity, although it does include elasticity and strain hardening. By Remark (1), this failure can only be ascribed to shortcomings in the way elasticity and/or strain hardening are accounted for in this model.

In view of the popularity of Gurson (1977)'s model for the description of the ductile behaviour of metals and alloys, it seems worth trying and improving it with respect to those two aspects, so as to adapt it better to the prediction of ductile rupture under cyclic loading conditions.

With respect to *strain hardening*, a first step in this direction was made by Leblond *et al.* (1995). Their work was based on the observation that as a result of Gurson (1977)'s overly simplified modelling of strain hardening, his model yielded predictions of the porosity evolution contradicting, to some extent, the results of micromechanical simulations. They proposed to improve the model by better accounting for the heterogeneous distribution of hardening within the hollow sphere considered (typical representative cell in a porous plastic material). The most notable change introduced consisted in introducing

[1] This is due to a somewhat paradoxical effect of *reversibility of plastic flows* in such materials, analogous to the reversibility of Stokes (extremely viscous) flows in fluid mechanics.

two (scalar) parameters characterizing (isotropic) hardening, instead of *one* like in Gurson (1977)'s original model; this revealed essential for the correct reproduction of some features of the porosity evolution.

Although Leblond *et al.* (1995)'s work was not directly concerned with cyclic loadings, their improved variant of Gurson (1977)'s model was tentatively applied by Devaux *et al.* (1997) to the prediction of the porosity evolution under such conditions. The results were mitigated: the improved Gurson-like model revealed free of the drawback of Gurson (1977)'s original version evidenced by Devaux *et al.* (1997) and mentioned in Point (2) above, but did not accurately predict the ratcheting of the porosity observed in micromechanical simulations. Lacroix *et al.* (2016) ascribed this somewhat disappointing result to some hypothesis of positively proportional straining made in Devaux *et al.* (1997)'s model, obviously quite unfit to cyclic loadings for which the components of the overall strain rate change sign every half-cycle. They proposed a further improvement of the model by dropping this hypothesis, at the expense of introduction, at each "macroscopic material point", of some underlying hollow sphere (typical elementary cell) discretized into a number of spherical layers; each layer having its own (isotropic) hardening variable, updated and stored at each time-step. The agreement between theoretical and numerical porosity evolutions then became much better, provided micromechanical simulations used a very high value of Young's modulus aimed at almost suppressing the effect of elasticity.

A new avenue to the modelling of strain hardening effects in porous plastic materials was recently opened by Morin *et al.* (2017). These authors' work was based on use of the so-called theory of sequential limit-analysis, as introduced from a purely numerical point of view by Yang (1993), then applied to various problems by Corradi and Panzeri (2004); Leu (2007); Leu and Li (2012); Kong *et al.* (2017); Yuan *et al.* (2017), among others, and finally analyzed theoretically by Leblond *et al.* (2018). This theory permitted to extend the methods and results of classical limit-analysis (Hill, 1951; Drucker *et al.*, 1952) by accounting for strain hardening and geometry changes, at the expense of neglect of elasticity.[2] Its application in the work of Morin *et al.* (2017) permitted to (i) justify (with the hypothesis of negligible elasticity) Lacroix *et al.* (2016)'s "spherical layer model"; and (ii) extend it to more complex hardening rules involving kinematic hardening. The quality of the instantaneous overall yield surfaces predicted were compared to those obtained through numerical limit-analyses of hollow spheres with prescribed distributions of pre-hardening, with favorable results. However, Morin *et al.* (2017) did not consider complex kinematic hardening rules including cyclic effects; nor did they perform micromechanical simulations of the evolution in time of hollow cells, as is necessary to assess the applicability of the model to cyclic loadings.

Much less has been done on the study and modelling of the influence of *elasticity* upon cyclic ductile rupture. From the point of view of micromechanical simulations, although this influence was noted some 25 years ago by Devaux *et al.* (1997), it was somewhat forgotten until Mbiakop *et al.* (2015), and even more Cheng *et al.* (2017), stressed its importance again. From the theoretical point of view, the situation is more difficult than

[2] The situation is different from that in classical limit-analysis (in the absence of strain hardening and within a geometrically linearized context), where the disregard of elasticity at limit-loads is rigorously justified; see (Drucker *et al.*, 1952).

for the influence of strain hardening, since the theory of sequential limit-analysis willfully ignores elasticity (Leblond *et al.*, 2018), and thus cannot be used to study or model its effect. However an interesting proposal to account for this effect, apparently the first of its kind, was recently made by Cheng *et al.* (2017). It consisted of "decoupling" elasticity and (visco)plasticity, by using linear and nonlinear homogenization theories to approximately evaluate the overall elastic and (visco)plastic potentials, separately and independently. This basically amounted to simply adding (within a Eulerian context) the (hypo)elastic and (visco)plastic deformation rates, without accounting for their possible interactions. Although appealing in principle, and indeed able to reproduce the results of some micromechanical simulations (Cheng *et al.*, 2017), this proposal by definition ignores the impact of the elastic deformation upon the plastic strain rate, which we shall try and show here to be, in all probability, *the* major factor governing the impact of elasticity upon the ratcheting of the porosity under cyclic loadings.

The aim of this paper is to pursue the study and modelling of the effects of strain hardening and elasticity upon cyclic ductile rupture of porous plastic materials. Distinct, unrelated methods will be used to deal with these two aspects of the material behaviour - both in conjunction with micromechanical simulations:

- for the effect of hardening, Morin *et al.* (2017)'s approach based on sequential limit-analysis, coupled with micromechanical simulations with an artificially high value of Young's modulus so as to make elasticity negligible;
- for the effect of elasticity, an evolution equation of the porosity incorporating - apparently for the first time - elasticity, coupled with micromechanical simulations with a "normal" value of Young's modulus.

The organization of the paper follows this programme in a natural way:

- Section 2 first presents the microscopic hardening laws studied in the paper, including a complex one incorporating cyclic effects, not considered in Morin *et al.* (2017)'s previous work. Then, disregarding elasticity in a first step, it expounds the macroscopic model resulting from application of Morin *et al.* (2017)'s approach to the hardening laws considered.
- Section 3 expounds the results of micromechanical simulations of hollow spheres made of *quasi-rigid*-plastic materials obeying various hardening laws, and subjected to various cyclic loading conditions. The aim here is to assess the validity of the model developed in the preceding Section.
- As a prerequisite to the modelling of the effect of elasticity, Section 4 is devoted to the derivation of an evolution equation for the porosity including the effect of elasticity. This is done first within a geometrically linearized context, then within a fully general geometric framework, at the expense of some slight modification of the usual microscopic and macroscopic hypoelasticity laws.
- Section 5 finally develops a macroscopic constitutive model accounting for the influence of elasticity upon the porosity evolution through the equation derived in Section 4. Comparisons of the model predictions with results of micromechanical simulations performed for *elastic*-plastic materials are made; they reveal the necessity of use, in the overall yield criterion and plastic flow rule, of some "effective" porosity slightly differing from the true one through some heuristic parameter.

2 Microscopic and macroscopic constitutive laws

Throughout the paper, a large displacement / large strain formulation (no geometric linearization) will be employed, unless otherwise stated. Use will be made of the Eulerian strain rate $\mathbf{d}$ (symmetric part of the velocity gradient) and the Cauchy stress tensor $\boldsymbol{\sigma}$ (true, actual force divided by true, actual surface).

2.1 Local yield criterion, plastic flow rule and evolution of hardening parameters

The material considered is elastic-plastic and exhibits a mixed (isotropic+kinematic) hardening. Its yield criterion, of von Mises type, reads:

$$\phi(\boldsymbol{\sigma}) \equiv (\boldsymbol{\sigma}-\boldsymbol{\alpha})^2_{eq} - \overline{\sigma}^2 \leq 0 \quad , \quad (\boldsymbol{\sigma}-\boldsymbol{\alpha})_{eq} \equiv \left[\frac{3}{2}(\boldsymbol{\sigma}'-\boldsymbol{\alpha}) : (\boldsymbol{\sigma}'-\boldsymbol{\alpha})\right]^{1/2}, \tag{1}$$

where $\overline{\sigma}$ is the current yield stress, $\boldsymbol{\sigma}' \equiv \boldsymbol{\sigma} - \frac{1}{3}(\mathrm{tr}\,\boldsymbol{\sigma})\,\mathbf{1}$ ($\mathbf{1}$: second-order unit tensor) the deviator of $\boldsymbol{\sigma}$, and $\boldsymbol{\alpha}$ a traceless symmetric "backstress" tensor. The flow rule is "associated" to the criterion *via* the normality property adapted to metal plasticity:

$$\mathbf{d}^p = \dot{\lambda}\frac{\partial \phi}{\partial \boldsymbol{\sigma}}(\boldsymbol{\sigma}) = 3\dot{\lambda}(\boldsymbol{\sigma}'-\boldsymbol{\alpha}), \tag{2}$$

where $\mathbf{d}^p$ is the plastic strain rate and $\dot{\lambda}$ the plastic multiplier, obeying the Kuhn-Tucker conditions $\dot{\lambda} \geq 0$, $\dot{\lambda}\phi = 0$.

Isotropic hardening. This type of hardening is governed by the current value of the yield stress $\overline{\sigma}$. The simplest hypothesis consists of assuming it to be a given, increasing function of the cumulated plastic strain p :

$$\overline{\sigma} \equiv \overline{\sigma}(p) \quad , \quad p(t) \equiv \int_0^t d^p_{eq}(\tau)d\tau \quad , \quad d^p_{eq} \equiv \left(\frac{2}{3}\,\mathbf{d}^p : \mathbf{d}^p\right)^{1/2}. \tag{3}$$

This simple law does not account for complex cyclic effects. A more elaborate one - a simplified version of Chaboche (1991)'s classical model - is presented in Appendix A.

Kinematic hardening. The simplest model of kinematic hardening involves a linear evolution law for the backstress $\boldsymbol{\alpha}$:

$$\breve{\boldsymbol{\alpha}} = \frac{2}{3}\,C\mathbf{d}^p \tag{4}$$

where $\breve{\boldsymbol{\alpha}}$ denotes some objective time-derivative of $\boldsymbol{\alpha}$ - the usual choice being Jaumann's derivative - and C some constant homogeneous to a stress, representing the "hardening slope" in simple tension.

This model is crude since it involves a constant hardening slope. In order to account for the different slopes at the end of loading and the beginning of the plastic phase of unloading,

Armstrong and Frederick (2007) proposed a more elaborate evolution equation:

$$\breve{\boldsymbol{\alpha}} = \frac{2}{3} C \mathbf{d}^p - \gamma \boldsymbol{\alpha} \dot{p} \tag{5}$$

where γ is a positive, dimensionless "relaxation parameter". At constant plastic strain rate $\mathbf{d}^p$, this equation describes an exponential evolution of $\boldsymbol{\alpha}$ toward the stationary value $\frac{2}{3}\frac{C}{\gamma}\frac{\mathbf{d}^p}{\dot{p}}$; so that the stress-strain curve in simple tension is concave and goes to some horizontal asymptote for large strains.

More complex and realistic behaviours may be obtained by taking the backstress $\boldsymbol{\alpha}$ as a sum of kinematic variables $\boldsymbol{\alpha}_k$ obeying distinct Armstrong and Frederick (2007)-type evolution laws:

$$\boldsymbol{\alpha} = \sum_{k=1,K} \boldsymbol{\alpha}_k \quad ; \quad \breve{\boldsymbol{\alpha}}_k = \frac{2}{3} C_k \mathbf{d}^p - \gamma_k \boldsymbol{\alpha}_k \dot{p} \quad (k = 1, ..., K). \tag{6}$$

For instance, if one considers two kinematic variables $\boldsymbol{\alpha}_1$ and $\boldsymbol{\alpha}_2$, the first obeying a simple linear evolution rule ($C_1 \neq 0$, $\gamma_1 = 0$) and the second a rule including relaxation ($C_2 \neq 0$, $\gamma_2 \neq 0$), one gets a more realistic stress-strain curve in simple tension going to some *inclined* asymptote.

2.2 Principle of Morin et al. (2017)'s homogenization method

Morin *et al.* (2017) consider, as a typical "representative cell" in a porous material, a hollow sphere of internal radius a, external radius b, defining a porosity (void volume fraction) $f \equiv a^3/b^3$, subjected to conditions of homogeneous boundary strain rate (Mandel, 1964; Hill, 1967). The constitutive material is momentarily assumed to be plastic but devoid of elasticity, with local yield criterion and flow rule given by equations (1) and (2). For a given and fixed distribution of (isotropic and kinematic) hardening parameters, Morin *et al.* (2017) use the theory of sequential limit-analysis to derive an instantaneous overall yield criterion and flow rule.

In order to simplify the calculations required and the resulting model, Morin *et al.* (2017) introduce - following Lacroix *et al.* (2016) who themselves drew inspiration from a work of Hervé and Zaoui (1993) - a radial discretization of the hollow sphere defined by the $N + 1$ radii

$$a = r_1 < r_2 < ... < r_{N+1} = b \tag{7}$$

(Fig. 1). The thin spherical layer lying between radii r_i and r_{i+1} is denoted $\mathcal{L}_i$. Use is made of the following notation:

$$f_i \equiv \frac{r_i^3}{b^3} \quad (i = 1, ..., N + 1). \tag{8}$$

The following approximations pertaining to the distributions of the isotropic and kinematic hardening variables are then introduced:

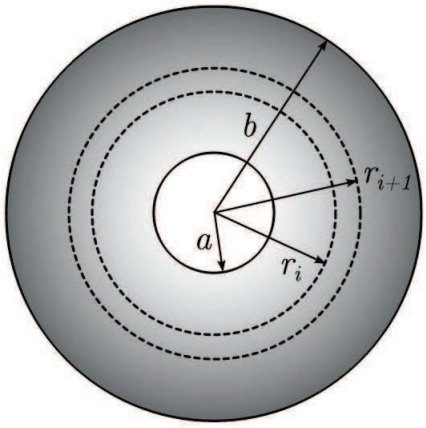

Fig. 1. Radial discretization of a hollow sphere.

(1) the yield stress $\overline{\sigma}$ is uniform within each layer $\mathcal{L}_i$, and denoted $\overline{\sigma}^i$ there;
(2) the distribution within layer $\mathcal{L}_i$ of the backstress $\boldsymbol{\alpha} \equiv \boldsymbol{\alpha}^i$ is of the form

$$\boldsymbol{\alpha}^i = \mathbf{A}_1^i + A_2^i \left(-2\mathbf{e}_r \otimes \mathbf{e}_r + \mathbf{e}_\theta \otimes \mathbf{e}_\theta + \mathbf{e}_\phi \otimes \mathbf{e}_\phi\right) \tag{9}$$

where $\mathbf{A}_1^i$ is a traceless symmetric tensor and A_2^i a scalar, both uniform within the layer, and $\mathbf{e}_r$, $\mathbf{e}_\theta$, $\mathbf{e}_\phi$ are the vectors of the orthonormal basis naturally associated to the spherical coordinates r, θ, ϕ.[3]

With these approximations, Morin *et al.* (2017) show that the overall plastic dissipation may be decomposed into two terms pertaining to the isotropic and kinematic parts of hardening respectively, both of which can be expressed as discrete sums over the layers $\mathcal{L}_i$. Then, from the expression of the overall dissipation, they deduce those of the overall yield criterion and flow rule.

It may be remarked here incidentally that Morin *et al.* (2017)'s method permits, among other things, to incorporate kinematic hardening into porous plasticity models in a much simpler and more natural way than previous heuristic approaches, proposed for instance by Mear and Hutchinson (1985) and Leblond *et al.* (1995).

2.3 Overall yield criterion and flow rule

The Gurson (1977)-type overall criterion derived by Morin *et al.* (2017) is of the form

$$\begin{aligned} \Phi(\boldsymbol{\Sigma}) \equiv \frac{(\boldsymbol{\Sigma} - \mathbf{A}_1)_{eq}^2}{\Sigma_1^2} + 2qf \cosh\left(\frac{3}{2}\frac{\Sigma_m - A_2}{\Sigma_2}\right) - 1 - q^2 f^2 \leq 0 \quad , \\ (\boldsymbol{\Sigma} - \mathbf{A}_1)_{eq} \equiv \left[\frac{3}{2}(\boldsymbol{\Sigma}' - \mathbf{A}_1) : (\boldsymbol{\Sigma}' - \mathbf{A}_1)\right]^{1/2} . \end{aligned} \tag{10}$$

[3] The form (9) of the $\boldsymbol{\alpha}^i$'s is compatible, via the evolution law (5) or (6) of these variables, with the form of Gurson (1977)'s trial velocity fields used in the limit-analysis: see Morin *et al.* (2017) and Subsection 2.4 below.

In this equation $\boldsymbol{\Sigma}$ denotes the macroscopic stress tensor, $\Sigma_m \equiv \frac{1}{3}\mathrm{tr}\,\boldsymbol{\Sigma}$ its mean part, $\boldsymbol{\Sigma}' \equiv \boldsymbol{\Sigma} - \Sigma_m \mathbf{1}$ its deviator; Σ_1 and Σ_2 are scalars together representing the isotropic part of macroscopic hardening; $\mathbf{A}_1$ and A_2 are a traceless symmetric tensor and a scalar, respectively, together defining some overall "backstress" representing the kinematic part of macroscopic hardening; and finally q denotes some heuristic dimensionless parameter of order unity, the introduction and value of which will be discussed in Subsection 3.2 below.

The macroscopic hardening parameters are given by the following discrete sums:

- for the isotropic part:

$$\begin{cases} \Sigma_1 = \dfrac{1}{1-f}\displaystyle\sum_{i=1}^{N} \overline{\sigma}^i \left(f_{i+1} - f_i\right) \\ \Sigma_2 = -\dfrac{1}{\ln f}\displaystyle\sum_{i=1}^{N} \overline{\sigma}^i \ln\left(\dfrac{f_{i+1}}{f_i}\right); \end{cases} \tag{11}$$

- for the kinematic part:

$$\begin{cases} \mathbf{A}_1 = \displaystyle\sum_{i=1}^{N} \mathbf{A}_1^i \left(f_{i+1} - f_i\right) \\ A_2 = 2\displaystyle\sum_{i=1}^{N} A_2^i \ln\left(\dfrac{f_{i+1}}{f_i}\right). \end{cases} \tag{12}$$

Also, the normality property being preserved in the sequential-limit-analysis-based homogenization (Leblond *et al.*, 2018), the overall flow rule reads

$$\mathbf{D}^p = \dot{\Lambda}\frac{\partial \Phi}{\partial \boldsymbol{\Sigma}}(\boldsymbol{\Sigma}) = \dot{\Lambda}\left[3\frac{\boldsymbol{\Sigma}' - \mathbf{A}_1}{\Sigma_1^2} + \frac{qf}{\Sigma_2}\sinh\left(\frac{3}{2}\,\frac{\Sigma_m - A_2}{\Sigma_2}\right)\mathbf{1}\right] \tag{13}$$

where $\mathbf{D}^p$ is the macroscopic plastic strain rate and $\dot{\Lambda}$ the overall plastic multiplier, obeying the Kuhn-Tucker conditions $\dot{\Lambda} \geq 0$, $\dot{\Lambda}\Phi = 0$.

2.4 Evolution of overall internal parameters

With the approximation of negligible elasticity made by sequential limit-analysis, the evolution of the porosity f is governed by the classical equation resulting from matrix incompressibility:

$$\dot{f} = 3(1-f)D_m^p \tag{14}$$

where $D_m^p \equiv \frac{1}{3}\mathrm{tr}\,\mathbf{D}^p$ denotes the macroscopic mean plastic strain rate.

Also, following Leblond *et al.* (1995), Lacroix *et al.* (2016) and Morin *et al.* (2017), in the evolution of the geometry, we account only for the hydrostatic part of the overall strain rate - a logical approximation insofar as the model developed is intended to be applied essentially to high triaxiality situations, for which void shape effects are negligible. With this approximation the initially spherical layers $\mathcal{L}_i$ remain spherical at all times, and the evolution equations of the radii r_i defining them read (accounting again for matrix

incompressibility):

$$\dot{r}_i = \frac{r_i}{f_i}\, D_m^p \quad (i = 1, ..., N+1). \tag{15}$$

Following Morin *et al.* (2017), the evolution equations of the hardening parameters are deduced from Gurson (1977)'s trial velocity fields used in the sequential limit-analysis and read, for every $i = 1, ..., N$:

- For the isotropic part:

$$\begin{aligned} p^i(t) = \int_0^t \dot{p}^i(\tau) d\tau \quad , \quad \dot{p}^i = \left(D_{eq}^{p\,2} + 4\frac{b^6}{\overline{r}_i^6}\, D_m^{p\,2} \right)^{1/2} \quad , \\ D_{eq}^p \equiv \left(\frac{2}{3}\, \mathbf{D}^{p\prime} : \mathbf{D}^{p\prime} \right)^{1/2} \quad , \quad \overline{r}_i \equiv \frac{1}{2}\,(r_i + r_{i+1}) \end{aligned} \tag{16}$$

  where $\mathbf{D}^{p\prime} \equiv \mathbf{D}^p - D_m^p \mathbf{1}$ denotes the deviator of $\mathbf{D}^p$;
  · for the simple "monotonic model" defined by equation (3):

$$\overline{\sigma}^i = \overline{\sigma}(p^i); \tag{17}$$

  · for the variant of Chaboche (1991)'s "cyclic model" presented in Appendix A:

$$\begin{cases} \overline{\epsilon}^i(t) & \equiv \displaystyle\int_0^t \mathrm{sgn}[\mathrm{tr}\,\mathbf{D}(\tau)]\dot{p}^i(\tau) d\tau \\ \overline{\epsilon}^i_{\max}(t) & \equiv \displaystyle\max_{0\le\tau\le t} \overline{\epsilon}^i(\tau) \\ \overline{\epsilon}^i_{\min}(t) & \equiv \displaystyle\min_{0\le\tau\le t} \overline{\epsilon}^i(\tau) \\ q^i & \equiv \frac{1}{2}\,(\overline{\epsilon}^i_{\max} - \overline{\epsilon}^i_{\min}) \\ \dfrac{d\overline{\sigma}^i}{dt} & = B\left[Q(q^i) - \overline{\sigma}^i \right] \dot{p}^i \end{cases} \tag{18}$$

  with the initial condition $\overline{\sigma}^i(t=0) = \sigma_0$; the symbol $\mathbf{D}$ in equation $(18)_1$ represents the macroscopic total strain rate.
- For the kinematic part:

$$\begin{cases} \mathbf{A}_1^i = \displaystyle\sum_{k=1,K} \mathbf{A}_{1k}^i \quad , \quad \breve{\mathbf{A}}_{1k}^i = \frac{2}{3}\, C_k \mathbf{D}^{p\prime} - \gamma_k \mathbf{A}_{1k}^i\, \dot{p}^i \\ A_2^i = \displaystyle\sum_{k=1,K} A_{2k}^i \quad , \quad \dot{A}_{2k}^i = \frac{2}{3}\, C_k \frac{b^3}{\overline{r}_i^3} D_m^p - \gamma_k A_{2k}^i\, \dot{p}^i \end{cases} \quad , \quad (k = 1, ..., K); \tag{19}$$

  note that for every value of k, the kinematic variable $\boldsymbol{\alpha}_k$ is assumed here to evolve according to Armstrong and Frederick (2007)'s law $(6)_2$; however a simpler linear evolution law may be recovered by merely setting $\gamma_k = 0$.

3 Micromechanical simulations disregarding elasticity

3.1 Principle of the simulations

The finite element simulations presented in this paper stand as extensions of those performed by Lacroix *et al.* (2016) for isotropic hardening to other, more complex types of hardening. They are all based on consideration of a hollow representative cell Ω initially assuming the shape of a thick spherical shell (Fig. 2). The ratio of the initial inner to outer radii is 0.1 so that the initial porosity is $f_0 = 10^{-3}$.

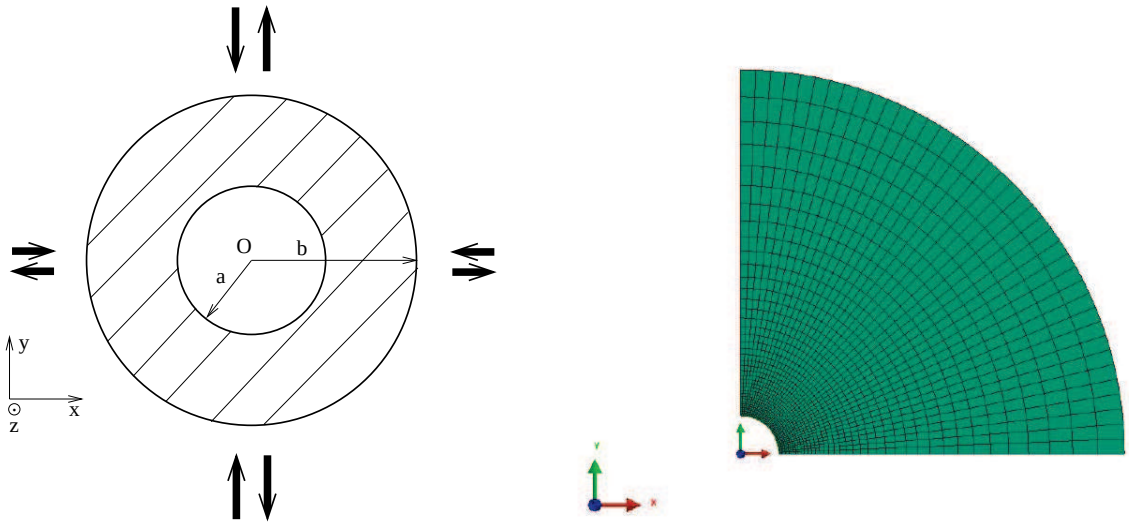

(a) Principle of simulations (b) Mesh in the initial configuration

Fig. 2. Principle of finite element micromechanical simulations and mesh of the initial hollow sphere.

All calculations are performed with a large displacement/large strain option, the cell being subjected to conditions of homogeneous boundary strain rate (Mandel, 1964; Hill, 1967) with an axisymmetric loading of axis Oy:

$$\mathbf{v}(\mathbf{x}) = \mathbf{D}.\mathbf{x} \quad \forall \mathbf{x} \in \partial\Omega \quad , \quad D_{xx} = D_{zz} \neq D_{yy} \, , \text{ other } D_{ij} = 0 \tag{20}$$

where $\mathbf{v}$ denotes the velocity and $\mathbf{x}$ the current position-vector. The ratio of the nonzero components $D_{xx} = D_{zz}$ and D_{yy} of the overall strain rate $\mathbf{D}$ is adjusted at each time-step so as to achieve a constant absolute value of the triaxiality

$$T \equiv \frac{\Sigma_m}{\Sigma_{eq}} \quad , \quad \Sigma_{eq} \equiv \left(\frac{3}{2} \boldsymbol{\Sigma}' : \boldsymbol{\Sigma}' \right)^{1/2} . \tag{21}$$

(Note that T changes sign from one half-cycle to the next one, since Σ_m changes sign whereas Σ_{eq} remains positive; thus the loading is proportional but *not* positively proportional).

We shall study the evolution of the porosity as a function of the *algebraic overall equivalent*

strain $\overline{E}_{eq}$ defined by the formula

$$\overline{E}_{eq}(t) \equiv \int_0^t \mathrm{sgn}\left[\Sigma_m(\tau)\right] D_{eq}(\tau) d\tau \quad , \quad D_{eq} \equiv \left(\frac{2}{3}\mathbf{D}' : \mathbf{D}'\right)^{1/2} \tag{22}$$

where $\mathbf{D}' \equiv \mathbf{D} - \frac{1}{3}(\mathrm{tr}\,\mathbf{D})\mathbf{1}$ is the deviator of the total strain rate $\mathbf{D}$. Each cycle is composed of a "tensile" half-cycle ($\Sigma_m > 0, T > 0$) during which $\overline{E}_{eq}$ increases from 0 to some prescribed, fixed value $\overline{E}_{eq}^{\max}$, followed by a "compressive" half-cycle ($\Sigma_m < 0, T < 0$) during which $\overline{E}_{eq}$ decreases back from $\overline{E}_{eq}^{\max}$ to 0.

In practice, the values of the loading parameters considered are $|T| = 2$ and 3, and $\overline{E}_{eq}^{\max} = 0.1$. Four cycles are simulated in each case considered.

The values of the elastic constants used are E (Young's modulus) $= 1,500\,\mathrm{GPa}$ and ν (Poisson's ratio) $= 0.3$. The artificially enhanced value of Young's modulus is intended to reduce the effect of elasticity as far as possible, so as to match the hypothesis of negligible elasticity made by sequential limit-analysis, the basis of the model presented above. The values of the plastic parameters differ from one case to another and will be given below.

All calculations are performed using the SYSTUS© commercial finite element code developed by ESI Group.

3.2 Choice of macroscopic model parameters

- **Choice of Tvergaard (1981)'s parameter** q. The heuristic parameter q in the macroscopic yield criterion (10) and flow rule (13) was introduced by Tvergaard (1981) in order to improve the agreement of model predictions and results of various micromechanical numerical simulations. He interpreted the non-unity value of q found (of the order of 1.5) as resulting from the use, in these simulations, of cell geometries differing from, and physically more realistic than, the spherical geometry considered by Gurson (1977). But the simulations presented here also precisely use a spherical cell geometry; hence it would seem logical to discard the parameter q, or equivalently set it to unity, in the model predictions to be compared to the simulation results.

  However, even taking for granted Gurson (1977)'s trial velocity fields for the spherical geometry, his treatment involved an additional approximation which induced further errors. This approximation was discussed and refined by Leblond and Morin (2014), with the conclusion that even for a spherical cell, a value of q slightly greater than unity, and depending upon the triaxiality, should be used. The values $q = 1.08$ for $|T| = 2$ and $q = 1$ for $|T| = 3$ were proposed by Lacroix *et al.* (2016) on the basis of Leblond and Morin (2014)'s results, and will be used in the comparisons to follow.
- **Choice of the number** N **of layers**. The number of spherical layers in the model is set to the value $N = 40$ (there are thus $N+1 = 41$ radii r_i). This choice is not arbitrary but precisely corresponds to the radial discretization adopted in the micromechanical simulations (see Fig. 2(b)).

3.3 Comparison of numerical results and model predictions for isotropic hardening

In this Subsection, like in (Lacroix *et al.*, 2016), we assume strain hardening to be of purely isotropic nature. (Note that the model discussed here then becomes exactly equivalent to that proposed by these authors). Hardening is assumed to correspond, again like in Lacroix *et al.* (2016)'s simulations, to the uniaxial stress-strain curve of the A508 Cl.3 steel used in the nuclear industry; see Fig. 3 in these authors' work. Figure 3 compares, for the triaxiality $|T| = 3$, the curves (f/f_0 vs. $\overline{E}_{eq}$) obtained numerically during the first four cycles to those predicted by the model. In this figure the symbol MM stands for "MicroMechanical simulation", and "$q = 1$" refers to the model predictions obtained with this value of Tvergaard (1981)'s parameter.

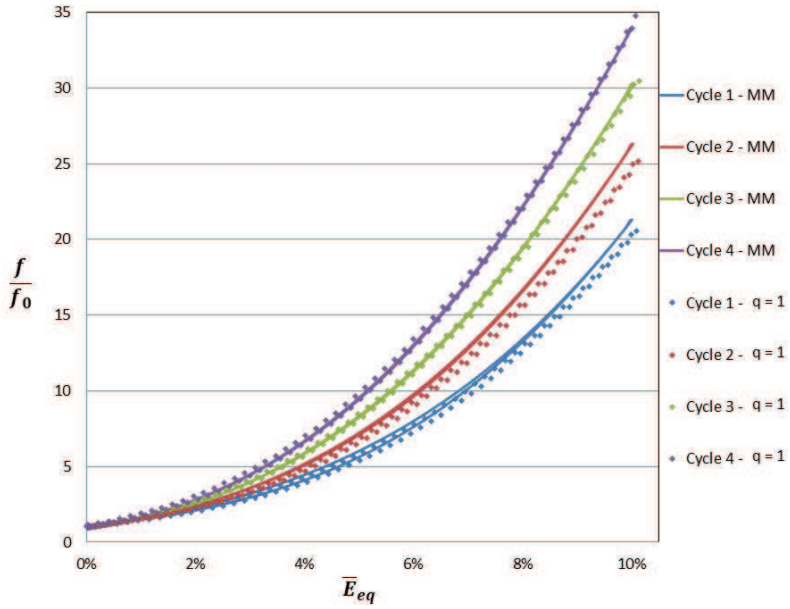

Fig. 3. Comparison of theoretical and numerical porosity evolutions - No elasticity - Isotropic hardening - $|T| = 3$.

Two points are noteworthy here:

- The numerical results are in excellent agreement with those of Lacroix *et al.* (2016), and in particular fully confirm the strong ratcheting of the porosity under cyclic loadings at high triaxialities.
- The close agreement of numerical and theoretical values of the porosity illustrates, again in line with Lacroix *et al.* (2016)'s findings, the quality of the "spherical layer model" for the type of hardening considered.

Figure 4 illustrates the corresponding mechanical behavior during the four cycles simulated: it provides the curves ($\Sigma_{yy} - \Sigma_{xx}$ vs. $\overline{E}_{eq}$), obtained numerically and predicted by the model. Note that $\Sigma_{yy} - \Sigma_{xx}$ is a kind of "algebraic equivalent stress" since $|\Sigma_{yy} - \Sigma_{xx}| = \Sigma_{eq}$.

The following points are noteworthy here:

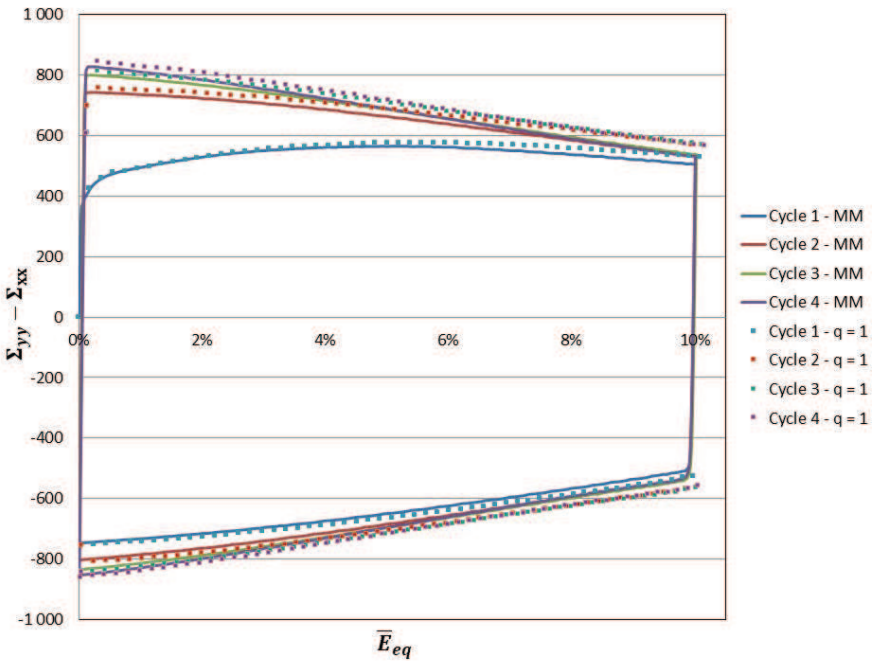

Fig. 4. (Algebraic equivalent stress)-(algebraic equivalent strain) - No elasticity - Isotropic hardening - $|T| = 3$.

- During the tensile phase of the first cycle, the algebraic equivalent stress first increases, obviously because of strain hardening, then decreases due to the increase of the porosity. During the tensile phase of later cycles, the algebraic equivalent stress only decreases, because the increase of the porosity takes precedence over strain hardening.
- In contrast, during the compressive phase of all cycles, the algebraic equivalent stress always decreases (increases in absolute value), because of the combined effects of strain hardening and the decrease of the porosity.
- From one cycle to the next, the material globally hardens (be it in tension or compression), which indicates that strain hardening is more globally important than the average increase of the porosity. It is clear, however, that the converse would become true for later cycles (not simulated here).
- The model makes a very good job of reproducing the numerical results.

We shall concentrate hereafter on the curves (f/f_0 vs. $\overline{E}_{eq}$), which provide the most important insights about the micromechanical simulations and the comparison of their results and model predictions.

3.4 Comparison of numerical results and model predictions for linear kinematic hardening

We now assume hardening to be of purely kinematic, linear type, with one variable $\boldsymbol{\alpha}_1$ having $C_1 = 1,500\,\text{MPa}$ and $\gamma_1 = 0$. Figure 5 shows the results obtained for $|T| = 2$.

The essential novelty here, apparent in both numerical results and model predictions (themselves in reasonable agreement), is the replacement of the ratcheting of the porosity

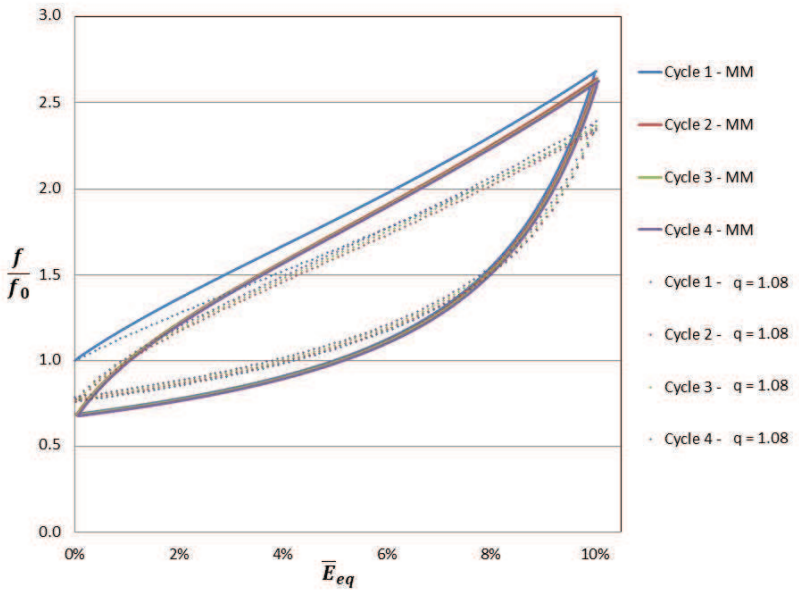

Fig. 5. Comparison of theoretical and numerical porosity evolutions - No elasticity - Linear kinematic hardening - $|T| = 2$.

by some almost instantaneous stabilization of the cyclic (F/f_0 vs. $\overline{E}_{eq}$) curve; the porosity decreases more in compression than it increases in tension, giving rise to "belly-shaped" cycles. This shows that the evolution of the porosity under cyclic loadings is a highly non-trivial feature that depends upon the *type* (isotropic/kinematic) of hardening.

It might be argued that the asymmetry found here between the "tension" and "compression" phases of the cyclic (F/f_0 vs. $\overline{E}_{eq}$) curve is of little practical importance, since the *maximum* value of the porosity is the same for all cycles. But this argument applies only to the "perfect" cycles considered here, for which the algebraic equivalent strain $\overline{E}_{eq}$ always oscillates between the same values 0 and $\overline{E}_{eq}^{\max}$; if the minimum and maximum values of $\overline{E}_{eq}$ varied with the cycle number, as is bound to frequently occur in practical cases, the presence of the "belly" in the stabilized cyclic (F/f_0 vs. $\overline{E}_{eq}$) curve would clearly have an important influence upon the succession of maximum values of f/f_0.

3.5 Comparison of numerical results and model predictions for kinematic hardening of Armstrong and Frederick (2007)'s type

We now consider the case of some kinematic Armstrong and Frederick (2007)-type hardening, with one variable $\boldsymbol{\alpha}_1$ having $C_1 = 1,500\,\text{MPa}$ and $\gamma_1 = 100$. Figure 6 illustrates the results obtained for $|T| = 2$.

One again observes a ratcheting of the porosity like in Fig. 3 for a purely isotropic hardening, although more modest here. (But the triaxiality is lower; note also that the agreement between numerical results and model predictions is less good). Comparison between the results presented in Subsection 3.4 and here, for the same value of C_1 but different values of γ_1, clearly shows that the qualitative behaviour of the porosity under cyclic loadings

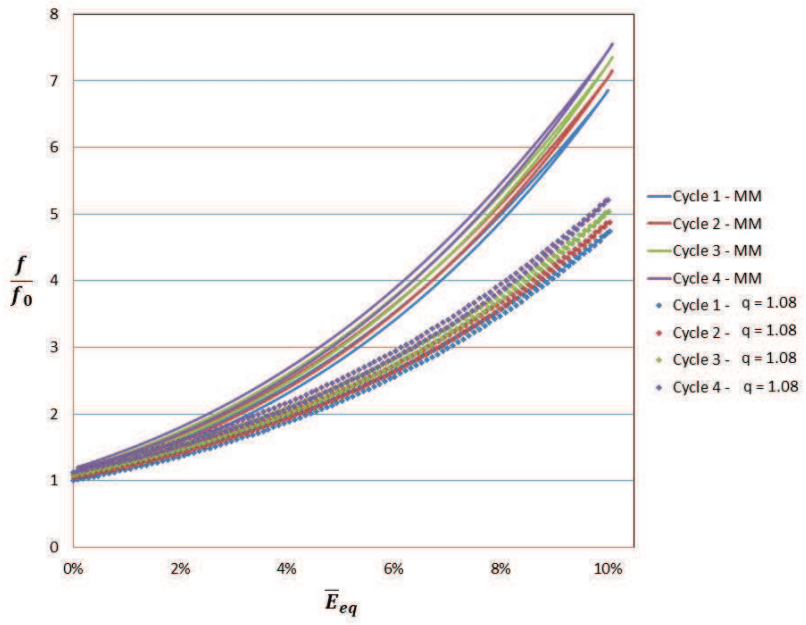

Fig. 6. Comparison of theoretical and numerical porosity evolutions - No elasticity - Nonlinear kinematic hardening - $|T| = 2$.

does not depend only on the *type* of hardening but also on the *values of the hardening parameters*.

3.6 Comparison of numerical results and model predictions for mixed isotropic/kinematic hardening

We finally consider a complex hardening model of the "simplified-Chaboche (1991)-type" involving cyclic effects, as described in Appendix A. The kinematic part of hardening is depicted with two variables, the first one, $\boldsymbol{\alpha}_1$, having $C_1 = 15,315\,\text{MPa}$ and $\gamma_1 = 1,965$, the second one, $\boldsymbol{\alpha}_2$, having $C_2 = 1,875\,\text{MPa}$ and $\gamma_2 = 0$ (linear hardening). These values are deduced from the first (unstabilized) cycles of cyclic stress-strain curves of the A508 Cl.3 steel. The function $Q(q)$, providing the stress amplitude Q of the stabilized cyclic stress-strain curves versus the strain amplitude, is approximately identified using the monotonic stress-strain curve of the same steel.[4] Note that the dependence of Q upon q, characteristic of the model envisaged, does play a role in both numerical results and theoretical predictions, since the strain amplitudes q^i in the various spherical layers $\mathcal{L}_i$ are different.

Figure 7 shows the results obtained for $|T| = 3$. A strong ratcheting of the porosity, reasonably well predicted by the model, may again be observed.

[4] This procedure involves some approximation since the set of "maximum points" of the stabilized cyclic curves differs from the monotonic stress-strain curve. This approximation is deemed acceptable insofar as our aim here is merely to provide an illustrative example, not to precisely reproduce the behaviour of a specific material.

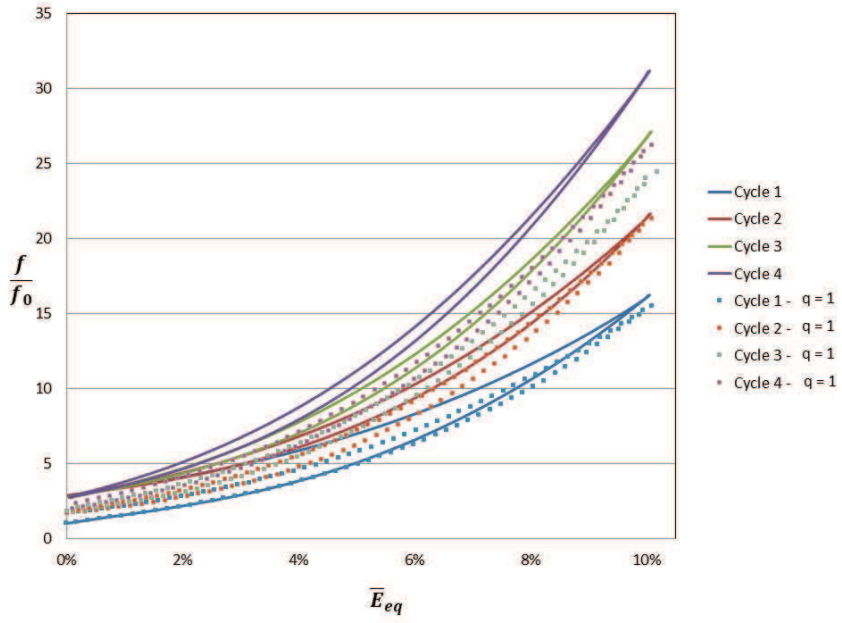

Fig. 7. Comparison of theoretical and numerical porosity evolutions - No elasticity - Mixed isotropic/kinematic hardening - $|T| = 3$.

4 An evolution equation of the porosity including elasticity

4.1 Preliminary considerations

All the micromechanical simulations presented in Section 3 used a value of Young's modulus of $1,500\,\mathrm{GPa}$, about 10 times larger than the standard value for a typical steel. This permitted to greatly reduce, if not completely eliminate, the effect of elasticity. But as mentioned in the Introduction, the existence of this effect was noted more than 25 years ago by Devaux *et al.* (1997), and emphasized again recently by Mbiakop *et al.* (2015) and Cheng *et al.* (2017). The simplest way of illustrating it is to consider an ideal-plastic material, so as to eliminate the effect of strain hardening, and compare simulations performed with standard and enhanced values of Young's modulus. Such a comparison is provided in Fig. 8, for the values $E = 1,500\,\mathrm{GPa}$ and $150\,\mathrm{GPa}$, and σ_0 (yield stress) $= 366\,\mathrm{MPa}$.

For the material having $E = 1,500\,\mathrm{GPa}$, almost devoid of elasticity, the ratcheting of the porosity is marginal. On the other hand, the ratcheting is clearly observable for the material having a standard value of Young's modulus, $E = 150\,\mathrm{GPa}$. This fully confirms the observations of Devaux *et al.* (1997), Mbiakop *et al.* (2015) and Cheng *et al.* (2017).

As mentioned in the Introduction, the work of Cheng *et al.* (2017) represents the sole previous attempt to incorporate such an effect into some macroscopic model. The procedure used, which consisted of evaluating separately and independently the overall elastic and (visco)plastic potentials, fundamentally meant *neglecting elastic-plastic interactions*.

Our interpretation is different. In our view, the effect of elasticity upon the ratcheting of the porosity *precisely arises from the elastic-plastic coupling*. Indeed this effect does

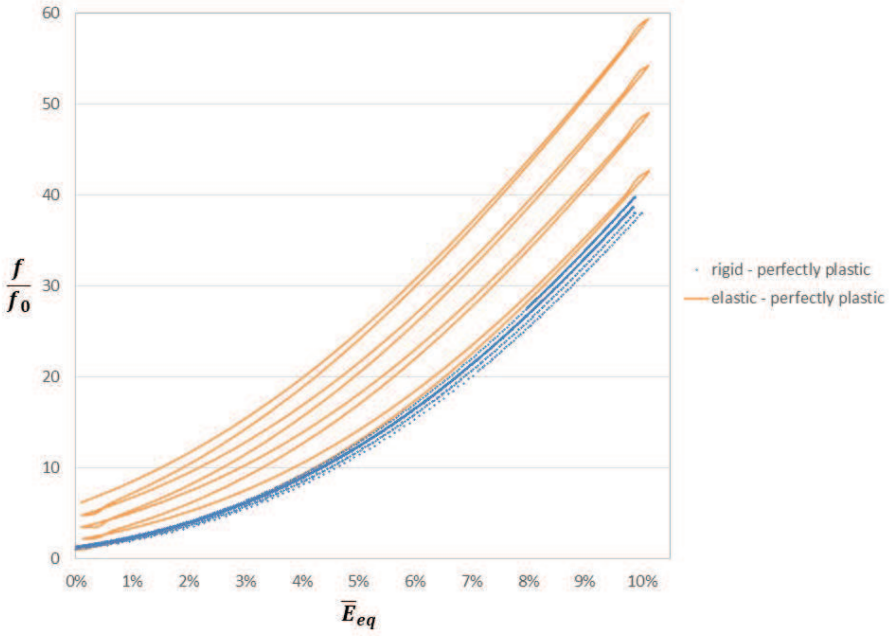

Fig. 8. Effect of elasticity upon the ratcheting of the porosity - $|T| = 3$.

not only occur during the purely elastic phase at the very beginning of each half-cycle, but during the entire subsequent plastic phase; indeed in Fig. 8, the gap between arcs of the (F/f_0 vs. $\overline{E}_{eq}$) curve corresponding to successive half-cycles continuously increases with time. Our idea is as follows: elasticity tends to slightly (and reversibly) enhance the porosity in tension, and reduce it in compression; since for a given mechanical state, the porosity rate is an increasing function of the porosity itself,[5] the slight (elastic) gap of porosity between tension and compression generates a slightly higher $|\dot{f}|$ in tension than in compression, whence the asymmetry between successive half-cycles.

Clearly, the only way to deal with such an effect in a rigorous manner would be to use a homogenization theory fully accounting for the elastic-plastic coupling. But, although such a theory is currently under development - see notably (Lahellec and Suquet, 2007; Idiart and Lahellec, 2016) - it is not mature enough today to provide explicit and simple results, usable in the present context. We shall therefore use a different approach basically relying upon a more precise evolution equation of the porosity accounting for the effect of elasticity.

4.2 Overall compressibility modulus of a hollow elastic sphere

The first task is to provide the overall elastic compressibility coefficient of a hollow sphere. We thus consider, within a geometrically linearized context, a hollow sphere of internal and external radii a and b defining a porosity $f \equiv a^3/b^3$, made of some purely elastic material with Young's modulus E and Poisson's ratio ν (see for instance Fig. 1, forgetting

[5] The expression of $\dot{f}$ is easily deduced by eliminating the plastic multiplier $\dot{\Lambda}$ between the mean and deviatoric parts of the flow rule (13), and using equation (14).

about the internal layers). This sphere is subjected to some purely hydrostatic loading so that the values of the radial stress and displacement on the outer boundary $r = b$ amount to $\sigma_{rr}(r = b) = \Sigma_m$ and $u_r(r = b) = E_m\, b$ respectively, where $\Sigma_m \equiv \frac{1}{3}\mathrm{tr}\,\mathbf{\Sigma}$ and $E_m \equiv \frac{1}{3}\mathrm{tr}\,\mathbf{E}$ denote the mean parts of the overall stress and strain tensors, $\mathbf{\Sigma}$ and $\mathbf{E}$.

The solution of this problem is classical and may be found in any textbook on elasticity; it leads to the following relation between Σ_m and E_m, or equivalently $\mathrm{tr}\,\mathbf{\Sigma}$ and $\mathrm{tr}\,\mathbf{E}$:

$$\Sigma_m = \alpha\,\frac{E}{1-2\nu}\,E_m \quad \Leftrightarrow \quad \mathrm{tr}\,\mathbf{\Sigma} = \alpha\,\frac{E}{1-2\nu}\,\mathrm{tr}\,\mathbf{E} \quad , \quad \alpha \equiv \frac{1-f}{1+\frac{1+\nu}{2(1-2\nu)}f}\,. \tag{23}$$

4.3 Evolution equation of the porosity including elasticity - Geometrically linearized framework

In order to facilitate the understanding of the reasoning, we first present it within a linearized geometric framework. We thus consider, within such a context, a representative volume element (RVE) Ω made of some elastic-*plastic* material with Young's modulus E and Poisson's ratio ν, containing some voids collectively denoted ω, and defining a porosity f. To lighten the notation, we denote a domain and its volume with the same symbol. Then, whatever the loading and its evolution in time, the rate of the total volume is given by

$$\begin{aligned}\dot\Omega &= \dot\omega + \frac{d}{dt}(\Omega-\omega) = \dot\omega + \int_{\Omega-\omega}\mathrm{tr}\,\dot{\boldsymbol\epsilon}\;d\Omega = \dot\omega + \int_{\Omega-\omega}\mathrm{tr}\,\dot{\boldsymbol\epsilon}^e\,d\Omega = \dot\omega + \int_{\Omega-\omega}\frac{1-2\nu}{E}\,\mathrm{tr}\,\dot{\boldsymbol\sigma}\;d\Omega \\ &= \dot\omega + \frac{1-2\nu}{E}\int_{\Omega}\mathrm{tr}\,\dot{\boldsymbol\sigma}\;d\Omega = \dot\omega + \frac{1-2\nu}{E}\,\Omega\,\langle\,\mathrm{tr}\,\dot{\boldsymbol\sigma}\,\rangle_\Omega = \dot\omega + \frac{1-2\nu}{E}\,\Omega\,\mathrm{tr}\,\dot{\mathbf{\Sigma}}\end{aligned}$$

where the incompressibility of plastic flow and the elasticity law have been used. Now assuming the overall elasticity law (23) to be valid for the RVE considered, we get from there

$$\dot\Omega = \dot\omega + \alpha\Omega\,\mathrm{tr}\,\dot{\mathbf{E}}^e \tag{24}$$

where $\mathbf{E}^e$ denotes the overall elastic strain.

Using the definition of the porosity, $f \equiv \omega/\Omega$, we get from equation (24):

$$\dot f = \frac{\dot\omega}{\Omega} - \frac{\omega}{\Omega^2}\,\dot\Omega = \frac{\dot\Omega}{\Omega} - \alpha\,\mathrm{tr}\,\dot{\mathbf{E}}^e - \frac{\omega}{\Omega^2}\,\dot\Omega = (1-f)\frac{\dot\Omega}{\Omega} - \alpha\,\mathrm{tr}\,\dot{\mathbf{E}}^e = (1-f)\,\mathrm{tr}\,\dot{\mathbf{E}} - \alpha\,\mathrm{tr}\,\dot{\mathbf{E}}^e,$$

that is finally since $\dot{\mathbf{E}} = \dot{\mathbf{E}}^e + \dot{\mathbf{E}}^p$ where $\mathbf{E}^p$ denotes the overall plastic strain:

$$\dot f = (1-f)\,\mathrm{tr}\,\dot{\mathbf{E}}^p + (1-f-\alpha)\,\mathrm{tr}\,\dot{\mathbf{E}}^e. \tag{25}$$

4.4 Evolution equation of the porosity including elasticity - General geometric framework

We now consider a general geometric context more appropriate for problems of ductile rupture. This implies replacing linearized strains, denoted with symbols $\boldsymbol\epsilon$ and $\mathbf{E}$, by

Eulerian strain rates, denoted with symbols $\mathbf{d}$ or $\mathbf{D}$.

- **Position of the problem**. Except for the change of notations just mentioned, the beginning of the reasoning is exactly the same as within a geometrically linearized framework:

$$\dot{\Omega} = \dot{\omega} + \frac{d}{dt}(\Omega - \omega) = \dot{\omega} + \int_{\Omega-\omega} \operatorname{tr} \mathbf{d}\; d\Omega = \dot{\omega} + \int_{\Omega-\omega} \operatorname{tr} \mathbf{d}^e\, d\Omega. \tag{26}$$

  Now use of the microscopic hypoelasticity law yields

$$\mathbf{d}^e = \frac{1+\nu}{E}\,\breve{\boldsymbol{\sigma}} - \frac{\nu}{E}(\operatorname{tr}\breve{\boldsymbol{\sigma}})\mathbf{1} \quad \Rightarrow \quad \operatorname{tr}\mathbf{d}^e = \frac{1-2\nu}{E}\operatorname{tr}\breve{\boldsymbol{\sigma}} = \frac{1-2\nu}{E}\operatorname{tr}\dot{\boldsymbol{\sigma}}$$

  where we have assumed that the objective derivative $\breve{}$ "respects the trace" ($\breve{\mathbf{X}} = \dot{\mathbf{X}}$; such is the case notably for Jaumann's derivative). Equation (26) then becomes

$$\dot{\Omega} = \dot{\omega} + \int_{\Omega-\omega} \frac{1-2\nu}{E}\operatorname{tr}\dot{\boldsymbol{\sigma}}\; d\Omega = \dot{\omega} + \frac{1-2\nu}{E}\int_{\Omega} \operatorname{tr}\dot{\boldsymbol{\sigma}}\; d\Omega = \dot{\omega} + \frac{1-2\nu}{E}\,\Omega\,\langle \operatorname{tr}\dot{\boldsymbol{\sigma}}\,\rangle_\Omega.$$

  But at this stage we are stuck, because although the macroscopic stress is simply the average of the microscopic stress, the same is not true of the corresponding stress *rates*, within the geometrically general context considered.

- **Relation between microscopic and macroscopic stress rates**. The first step in the search for a solution to this problem is to derive the exact relation between microscopic and macroscopic stress rates. We follow here the same lines as in Stolz (1987)'s thesis. Since $\frac{d}{dt}(d\Omega) = \operatorname{tr}\mathbf{d}\, d\Omega$,

$$\frac{d}{dt}\left(\int_\Omega \boldsymbol{\sigma}\, d\Omega\right) = \int_\Omega (\dot{\boldsymbol{\sigma}} + \boldsymbol{\sigma}\operatorname{tr}\mathbf{d})\, d\Omega$$

  so that

$$\begin{aligned}\dot{\boldsymbol{\Sigma}} = \frac{d}{dt}\langle\,\boldsymbol{\sigma}\,\rangle_\Omega &= \frac{d}{dt}\left(\frac{1}{\Omega}\int_\Omega \boldsymbol{\sigma}\, d\Omega\right) = \frac{1}{\Omega}\int_\Omega (\dot{\boldsymbol{\sigma}} + \boldsymbol{\sigma}\operatorname{tr}\mathbf{d})\, d\Omega - \frac{\dot{\Omega}}{\Omega^2}\int_\Omega \boldsymbol{\sigma}\, d\Omega \\ &= \langle\,\dot{\boldsymbol{\sigma}} + \boldsymbol{\sigma}\operatorname{tr}\mathbf{d}\rangle_\Omega - (\operatorname{tr}\mathbf{D})\langle\,\boldsymbol{\sigma}\,\rangle_\Omega\end{aligned}$$

  or equivalently

$$\dot{\boldsymbol{\Sigma}} + \boldsymbol{\Sigma}\operatorname{tr}\mathbf{D} = \langle\,\dot{\boldsymbol{\sigma}} + \boldsymbol{\sigma}\operatorname{tr}\mathbf{d}\rangle_\Omega. \tag{27}$$

  In particular, taking the trace of this equation yields

$$\operatorname{tr}\dot{\boldsymbol{\Sigma}} + (\operatorname{tr}\boldsymbol{\Sigma})(\operatorname{tr}\mathbf{D}) = \langle\,\operatorname{tr}\dot{\boldsymbol{\sigma}} + (\operatorname{tr}\boldsymbol{\sigma})(\operatorname{tr}\mathbf{d})\rangle_\Omega. \tag{28}$$

- **Solution of the problem**. Equation (27) suggests to introduce new objective derivatives of the stress tensors, defined by the formulae

$$\begin{cases} \dfrac{D\boldsymbol{\sigma}}{Dt} \equiv \breve{\boldsymbol{\sigma}} + \boldsymbol{\sigma}\operatorname{tr}\mathbf{d} \\ \dfrac{D\boldsymbol{\Sigma}}{Dt} \equiv \breve{\boldsymbol{\Sigma}} + \boldsymbol{\Sigma}\operatorname{tr}\mathbf{D}. \end{cases} \tag{29}$$

We now assume that *the microscopic hypoelasticity law does not involve Jaumann's usual derivative but the new derivative* $\frac{D}{Dt}$, so that it now reads

$$\mathbf{d}^e = \frac{1+\nu}{E}\,\frac{D\boldsymbol{\sigma}}{Dt} - \frac{\nu}{E}\left(\operatorname{tr}\frac{D\boldsymbol{\sigma}}{Dt}\right)\mathbf{1}. \tag{30}$$

Two remarks are in order here:

- The hypothesis made is permissible since the choice of an objective derivative of the stress tensor in a hypoelasticity law is essentially a matter of taste and convenience, in the absence of any compelling theoretical argument favouring one or another. (Note also that the difference between the derivatives $\breve{}$ and $\frac{D}{Dt}$ is small, since $\operatorname{tr}\mathbf{D}$ is always small in practice).
- Such a hypothesis is equivalent to assuming that the standard hypoelasticity law involving Jaumann's derivative does apply, but to the tensor $\boldsymbol{\sigma}/\rho$ where ρ denotes the volumic mass, rather than the tensor $\boldsymbol{\sigma}$ itself: see Stolz (1987).

Taking the trace of equation (30)and using the definition $(29)_1$ of the derivative $\frac{D\boldsymbol{\sigma}}{Dt}$, we get

$$\operatorname{tr}\mathbf{d}^e = \frac{1-2\nu}{E}\operatorname{tr}\frac{D\boldsymbol{\sigma}}{Dt} = \frac{1-2\nu}{E}\left[\operatorname{tr}\breve{\boldsymbol{\sigma}} + (\operatorname{tr}\boldsymbol{\sigma})(\operatorname{tr}\mathbf{d})\right] = \frac{1-2\nu}{E}\left[\operatorname{tr}\dot{\boldsymbol{\sigma}} + (\operatorname{tr}\boldsymbol{\sigma})(\operatorname{tr}\mathbf{d})\right] \tag{31}$$

where use has been made again of the assumption that the derivative $\breve{}$ respects the trace. With this relation, equation (26) becomes

$$\begin{aligned}\dot{\Omega} &= \dot{\omega} + \frac{1-2\nu}{E}\int_\Omega \left[\operatorname{tr}\dot{\boldsymbol{\sigma}} + (\operatorname{tr}\boldsymbol{\sigma})(\operatorname{tr}\mathbf{d})\right] d\Omega = \dot{\omega} + \frac{1-2\nu}{E}\,\Omega\left\langle \operatorname{tr}\dot{\boldsymbol{\sigma}} + (\operatorname{tr}\boldsymbol{\sigma})(\operatorname{tr}\mathbf{d})\right\rangle_\Omega \\ &= \dot{\omega} + \frac{1-2\nu}{E}\,\Omega\left[\operatorname{tr}\dot{\boldsymbol{\Sigma}} + (\operatorname{tr}\boldsymbol{\Sigma})(\operatorname{tr}\mathbf{D})\right]\end{aligned}$$

where equation (28) has been used.

We finally introduce the reasonable assumption[6] that equation (23), valid within a linearized geometric context, becomes in the general framework considered here:

$$\operatorname{tr}\frac{D\boldsymbol{\Sigma}}{Dt} = \operatorname{tr}\breve{\boldsymbol{\Sigma}} + (\operatorname{tr}\boldsymbol{\Sigma})(\operatorname{tr}\mathbf{D}) = \operatorname{tr}\dot{\boldsymbol{\Sigma}} + (\operatorname{tr}\boldsymbol{\Sigma})(\operatorname{tr}\mathbf{D}) = \alpha\,\frac{E}{1-2\nu}\operatorname{tr}\mathbf{D}^e\,. \tag{32}$$

Insertion of equation (32) into the preceding expression of $\dot{\Omega}$ yields

$$\dot{\Omega} = \dot{\omega} + \alpha\Omega\operatorname{tr}\mathbf{D}^e \tag{33}$$

which is analogous to equation (24). From this point, the reasoning is the same as within a geometrically linearized context and leads to an analogous result:

$$\dot{f} = (1-f)\operatorname{tr}\mathbf{D}^p + (1-f-\alpha)\operatorname{tr}\mathbf{D}^e. \tag{34}$$

Equation (34) calls for some comments:

[6] *Assumption* because a rigorous homogenization theory for *hypo*elasticity does not seem to exist at present.

- To the best of our knowledge, the reasonings above and the final result (34) represent the first attempt, within the context of the modelling of ductile rupture, to derive a more accurate evolution equation of the porosity accounting for the influence of elasticity.
- Equation (34) may look a bit strange at first sight, because it seems to imply that in a sound, purely elastic material ($f = 0$, $\mathbf{D}^p = \mathbf{0}$), elasticity will generate some porosity; this is not so however, because α is unity in such a case (see equation $(23)_3$).
- In the limit of an elastically incompressible material ($\nu = 1/2$), α is zero (see equation $(23)_3$) so that equation (34) reduces to $\dot{f} = (1-f)\,\mathrm{tr}\,\mathbf{D}$ where $\mathbf{D} = \mathbf{D}^e + \mathbf{D}^p$ is the total strain rate. The meaning of this result is that in the absence of any compressibility (elastic or plastic) of the material, the entire volumetric strain rate "goes" into void growth. In this specific case, the expression of the porosity rate may be obtained from a purely kinematic argument, without any reference to the constitutive law: indeed equation (33) simply becomes $\dot{\Omega} = \dot{\omega}$, and the expression of $\dot{f}$ results from there following the same lines as above.
- For an elastically compressible material ($\nu < 1/2$), the presence of the positive coefficient α, in the multiplicative factor $(1 - f - \alpha)$ of $\mathrm{tr}\,\mathbf{D}^e$ in equation (34), reduces the impact of the elastic strain rate upon the porosity rate. This is obviously because part of the total volumetric strain rate $\mathrm{tr}\,\mathbf{D}$ "goes" into the elastic volumetric strain rate of the material. In such a case the expression (34) of $\dot{f}$ cannot be obtained from a purely kinematic argument, as is clear from the presence of the elasticity-dependent coefficient α in this expression.
- The value of the coefficient α does not only depend upon the porosity and Poisson's ratio, but also on the geometry of the RVE used to evaluate it. The value given by equation $(23)_3$ corresponds to a hollow sphere, and would be different for instance for a macroscopically isotropic distribution of voids of arbitrary shape.

A question which naturally arises about the exact evolution equation (34) of the porosity pertains to the importance of the term proportional to $\mathbf{D}^e$ in the right-hand side: what kind of error does one make when neglecting it? This issue is best addressed by considering the special case of an *ideal-plastic* material, like in Subsection 4.1. If one neglects the term proportional to $\mathbf{D}^e$ in equation (34), it becomes identical to (14), and the whole model of Section 2 becomes equivalent to that of Gurson (1977) (without hardening). It is therefore prone to the same shortcoming (Remark (2) of the Introduction): it does not predict any ratcheting of the porosity under cyclic loadings at fixed (absolute value of the) triaxiality. But Figure 8 above clearly evidences the inadequacy of this prediction.

5 A model for the ratcheting of the porosity including elasticity

5.1 Introduction of some effective porosity into the model

We ascribed, in Subsection 4.1, the influence of elasticity upon cyclic ductile rupture to the elastic (reversible) enlargement or shrinkage of voids. Hence, in order to incorporate such an influence into some macroscopic model, the first, most natural idea is simply to replace the evolution equation (14) of the porosity disregarding elasticity through the

more accurate equation (34), all other elements of the model (expounded in Section 2) remaining unchanged.

The "improved" model thus defined was applied to the prediction of the porosity evolution for the same material (with $E = 150\,\mathrm{GPa}$, meaning non-negligible elasticity) and under the same cyclic loading conditions as in Fig. 8. The results - not shown here for space reasons - were *qualitatively*, but *not quantitatively*, in agreement with the results of micromechanical simulations shown in this figure: they did display some ratcheting of the porosity but underestimated it.

This mitigated result is perhaps less surprising that it may seem at first sight. Indeed, simply adopting a more refined evolution of the porosity incorporating elasticity, basically means accepting the overall yield criterion and flow rule derived from sequential limit-analysis, using merely a more accurate estimate of the porosity. But, as mentioned in the Introduction, the theory and methods of sequential limit-analysis are precisely entirely based on the neglect of elasticity. Hence there is no reason why its results should be applicable in the presence of elasticity, with only such a minor adjustment.

In the absence, as of today, of some rigorous and practically usable homogenization method for elastic-(visco)plastic materials fully incorporating the elastic-plastic coupling, the only possibility left is to adopt a heuristic approach. Our proposal here is to accept, even in the presence of elasticity, the overall yield criterion (10) and plastic flow rule (13) derived from sequential limit-analysis, but with some "effective" porosity $\bar{f}$ slightly differing from the true one, f; this criterion and flow rule thus become:

$$\begin{cases} \Phi(\boldsymbol{\Sigma}) \equiv \dfrac{(\boldsymbol{\Sigma}-\mathbf{A}_1)^2_{eq}}{\Sigma_1^2} + 2q\bar{f}\cosh\left(\dfrac{3}{2}\dfrac{\Sigma_m - A_2}{\Sigma_2}\right) - 1 - q^2\bar{f}^2 \leq 0 \\ \mathbf{D}^p \quad = \dot{\Lambda}\dfrac{\partial\Phi}{\partial\boldsymbol{\Sigma}}(\boldsymbol{\Sigma}) = \dot{\Lambda}\left[3\dfrac{\boldsymbol{\Sigma}'-\mathbf{A}_1}{\Sigma_1^2} + \dfrac{q\bar{f}}{\Sigma_2}\sinh\left(\dfrac{3}{2}\dfrac{\Sigma_m - A_2}{\Sigma_2}\right)\mathbf{1}\right]. \end{cases} \tag{35}$$

All other equations defining the model are unchanged, including those involving the porosity which remains the true one, f.

The effective porosity $\bar{f}$ is defined as follows. First, the true porosity f is decomposed into plastic and elastic contributions, as suggested by the evolution equation (34):

$$f \equiv f^p + f^e \tag{36}$$

where the plastic part f^p and elastic part f^e of the porosity obey the following evolution equations and initial conditions:

$$\begin{cases} \dot{f}^p = (1-f)\,\mathrm{tr}\,\mathbf{D}^p & \text{with} \quad f^p(t=0) = f_0 \\ \dot{f}^e = (1-f-\alpha)\,\mathrm{tr}\,\mathbf{D}^e & \text{with} \quad f^e(t=0) = 0. \end{cases} \tag{37}$$

(The initial condition for f^e is logical insofar as the material is assumed to be stress-free initially). The effective porosity $\bar{f}$ is then defined as

$$\bar{f} \equiv f^p + \beta f^e \tag{38}$$

where β is an empirical parameter which may depend upon the (true) porosity.

A final remark about the model just defined is that it includes the effect of elasticity during all phases of the mechanical history - as is necessary to properly account for interactions between elasticity and plasticity - *including the purely elastic phase* at the very beginning of each semi-cycle. Note however that the approximation is made that all points of the RVE are simultaneously elastic or plastic (since we use a "global" yield criterion for the entire RVE), thus disregarding the gradual expansion of the plastic zone within it.

5.2 Comparison of model predictions and results of micromechanical simulations incorporating elasticity

Upon comparison of model predictions and results of micromechanical simulations for various types of hardening, it is found that these results are best reproduced using the following heuristic formula for the parameter β:

$$\beta = 1 + 11.5 \ \exp\left(-\frac{1}{4}\frac{f}{f_0}\right). \tag{39}$$

Figures 9, 10 and 11 illustrate the comparison between model predictions (with formula (39) for β) and results of micromechanical simulations, in the presence of elasticity ($E =$ 150 GPa), for three types of hardening: in Fig. 9, ideal plasticity with σ_0 (yield stress) $=$ 366 MPa like in Figure 8; (b) in Fig. 10, isotropic hardening with the same uniaxial stress-strain curve as in Figure 3; (c) in Fig. 11, Armstrong and Frederick (2007)-type kinematic hardening, with two variables having $C_1 = 15,315$ MPa and $\gamma_1 = 1,965$, and $C_2 = 1,875$ MPa and $\gamma_2 = 0$ (same parameters as in Figure 7, but without Chaboche (1991)'s modelling of complex cyclic effects). (In the last case it revealed difficult to perform micromechanical simulations for $|T| = 3$ so the slightly lower value $|T| = 2.5$ was adopted; Tvergaard (1981)'s parameter q was nevertheless set to unity like for the value $|T| = 3$). The agreement between model predictions and numerical results is quite acceptable in all three cases.

A final remark is in order here. It may seem tempting to use the numerical results presented to propose a classification of the effects of elasticity, isotropic and kinematic hardening, according to the importance of their impact upon the ratcheting of the porosity under cyclic loadings. In the authors' view, this temptation should be resisted for the following reasons: (i) our numerical results were not all obtained for the same (absolute value of the) triaxiality; (ii) the relative importance of the various effects totally depends upon the values of the constitutive parameters (elasticity coefficients, hardening parameters).

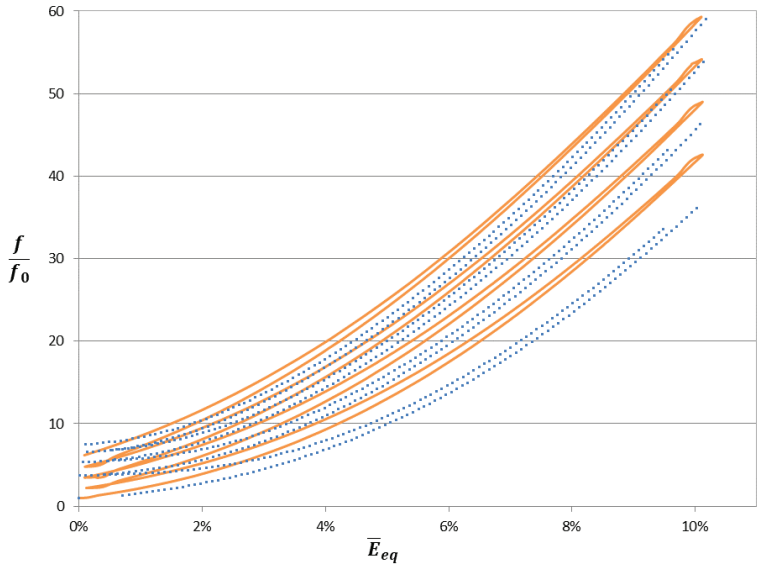

Fig. 9. Comparison of theoretical and numerical porosity evolutions - With elasticity - Ideal plasticity - $|T| = 3$.

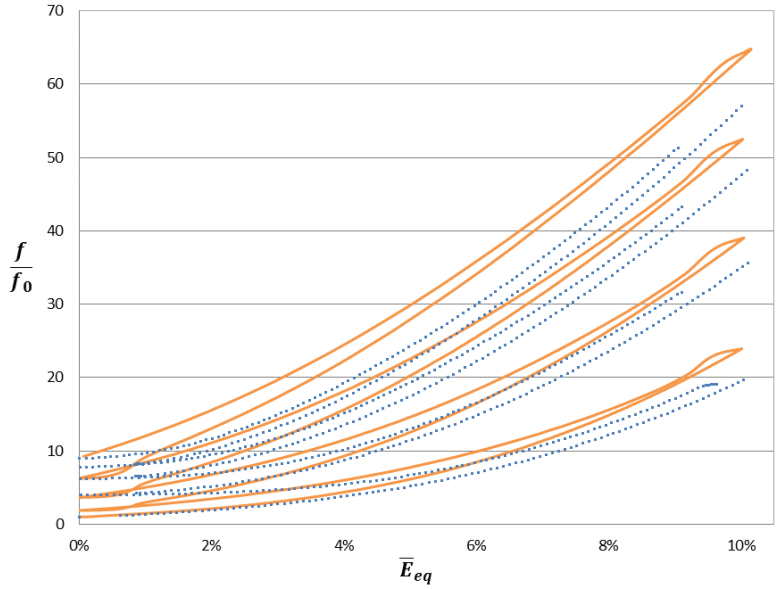

Fig. 10. Comparison of theoretical and numerical porosity evolutions - With elasticity - Isotropic hardening - $|T| = 3$.

6 Conclusion

This paper was devoted to the theoretical and numerical study of cyclic ductile rupture, with special emphasis upon the two features of the microscopic mechanical behaviour responsible for the so-called *ratcheting of the porosity*: namely *strain hardening* and *elasticity*. Distinct theoretical approaches were used to deal with these two phenomena.

In order to incorporate the influence of *strain hardening* upon the behaviour of ductile

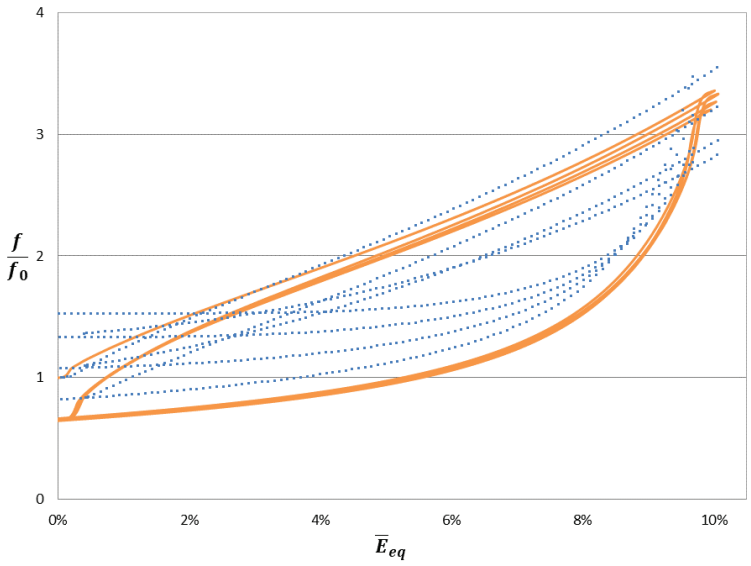

Fig. 11. Comparison of theoretical and numerical porosity evolutions - With elasticity - Nonlinear kinematic hardening - $|T| = 2.5$.

solids under cyclic loadings, we used the so-called theory of sequential analysis. This new kind of limit-analysis was introduced by Yang (1993), applied to homogenization of porous plastic solids by Morin *et al.* (2017), and finally analyzed and justified theoretically by Leblond *et al.* (2018). It extends the classical theory of limit-analysis of Hill (1951) and Drucker *et al.* (1952) by accounting for strain hardening and geometry changes; but it is fundamentally based - as demonstrated in detail by Leblond *et al.* (2018) - upon neglect of elasticity, and thus cannot account for this aspect of the mechanical behaviour.

We first recalled, in Section 2, Morin *et al.* (2017)'s results obtained through combination of sequential limit-analysis and homogenization of porous plastic (hardenable) solids. These results were then applied to more complex hardening laws. The types of hardening considered included (i) isotropic hardening; (ii) linear kinematic hardening; (iii) Armstrong and Frederick (2007)-type nonlinear kinematic hardening; and (iv) some simplified version of Chaboche (1991)'s mixed (isotropic+kinematic) hardening model including complex cyclic effects.

Section 3 was then devoted to the comparison of model predictions and results of some micromechanical simulations of hollow spheres, made of *rigid*-plastic materials with various hardening laws, and subjected to cyclic loadings under conditions of high and constant absolute value of the triaxiality. The (quasi-)absence of elasticity was accounted for in the simulations by using a very high (unrealistic) value for Young's modulus. The agreement of model predictions and numerical results for the evolution of the porosity was found to be acceptable in all cases investigated, and quite good in most of them. Also, an interesting finding was that a ratcheting of the porosity is not the only possibility for ductile solids subjected to cyclic loadings: depending upon the type of hardening and the values of hardening parameters, one may observe either such a ratcheting, *or* some "belly-shaped" aspect of the cycles in the cyclic porosity/overall strain curve.

The treatment of the effect of *elasticity* upon the cyclic ductile behaviour was based

on a quite different approach, making use of some more accurate evolution law of the porosity incorporating - apparently for the first time - the (reversible) influence of elastic deformations. In Section 4, such a law was first derived on fully rigorous grounds within a geometrically linearized framework. It was then extended to some fully general geometric context, using a few (unfortunately unavoidable but reasonable) hypotheses.

The results derived in Section 4 were finally used in Section 5 to define a refined model for porous ductile solids incorporating the influence of elasticity upon the cyclic behaviour. The first and most natural idea, consisting of simply replacing the usual evolution law of the porosity disregarding the effect of elasticity through the more accurate one including it, was found to yield qualitatively acceptable, but quantitatively unacceptable predictions for the ratcheting of the porosity under cyclic loadings. This was interpreted as a consequence of the basic inapplicability of sequential limit-analysis in the presence of elasticity. The heuristic remedy adopted consisted of using, in the overall yield criterion and plastic flow rule obtained through sequential limit-analysis, some "effective" porosity slightly differing from the true one through some phenomenological, adjustable parameter. With this modification, the agreement between model predictions and results of micromechanical simulations performed with a standard value of Young's modulus were found to be quite acceptable in all cases considered.

Apart from numerical applications to prediction of ductile rupture in actual structures loaded cyclically (as initiated in Remmal (2021)'s thesis), future developments will essentially focus on the case of cyclic loadings at lower triaxialities. Under such conditions void shape effects - completely disregarded in the present work - are bound to become important. Developing a model for the cyclic ductile behaviour under such general loadings will require combining the methods and results of the present paper with those used in earlier works (Madou and Leblond, 2012a,b, 2013; Madou *et al.*, 2013) to account for *ellipsoidal*, instead of *spherical* voids.

Acknowledgement

The authors wish to express their sincere thanks to the FRAMATOME Company, and especially Drs. Stéphane Chapuliot and Gilles Perrin, for their continued moral and financial support of this work.

References

Armstrong P. and Frederick C. (2007). A mathematical representation of the multiaxial Bauschinger effect, *Mater. High Temper.*, **24**, 11-26.

Besson J. and Guillemer-Neel C. (2003). An extension of the Green and Gurson models to kinematic hardening, *Mech. Mater.*, **35**, 1-18.

Brocks W. and Steglich D. (2003). Damage models for cyclic plasticity, in: *Key Engineering Materials*, vols. 251-252, pp. 389-398.

Chaboche J.L. (1991). On some modifications of kinematic hardening to improve the description of ratcheting effects, *Int. J. Plast.*, **7**, 661-678.

Cheng L., Danas K., Constantinescu A. and Kondo D. (2017). A homogenization model

for porous ductile solids under cyclic loads comprising a matrix with isotropic and linear kinematic hardening, *Int. J. Solids Structures*, **121**, 174-190.

Corradi L. and Panzeri N. (2004). A triangular finite element for sequential limit analysis of shells, *Adv. Engng. Software*, **35**, 633-643.

Devaux J., Gologanu M., Leblond J.B. and Perrin G. (1997). On continued void growth in ductile metals subjected to cyclic loadings, in: *Proceedings of the IUTAM Symposium on Nonlinear Analysis of Fracture*, Cambridge, GB, J. Willis, ed., Kluwer, pp. 299-310.

Drucker D.C., Prager W. and Greenberg M.J. (1952). Extended limit-analysis theorems for continuous media, *Quart. Appl. Math.*, **9**, 381-389.

Gilles Ph., Jullien B. and Mottet G. (1992). Analysis of cyclic effects on ductile tearing strength by a local approach of fracture, in: *Advances in Fracture/Damage Models for the Analysis of Engineering Problems*, ASME Publication AMD - Vol. 137, pp. 269-284.

Gurson A.L. (1977). Continuum theory of ductile rupture by void nucleation and growth: Part I - Yield criteria and flow rules for porous ductile media, *ASME J. Engng. Mater. Technol.*, **99**, 2-15.

Hervé E. and Zaoui A. (1993). N-layered inclusion-based micromechanical modelling, *Int. J. Engng. Sci.*, **31**, 1-10.

Hill R. (1951). On the state of stress in a plastic-rigid body at the yield point, *Phil. Mag.*, **42**, 868-875.

Hill R. (1967). The essential structure of constitutive laws for metal composites and polycrystals, *J. Mech. Phys. Solids*, **15**, 79-95.

Idiart M. and Lahellec N. (2016). Estimates for the overall linear properties of pointwise heterogeneous solids with application to elasto-viscoplasticity, *J. Mech. Phys. Solids*, **97**, 317–332.

Kobayashi H., Kusumoto T. and Nakazawa H. (1992). The cyclic J-R curve and upper limit characteristic of fatigue crack growth in 2-1/2 Cr-Mo steel, *Int. J. Press. Vessels Pip.*, **52**, 337-356.

Kong D., Martin C.M. and Byrne B.W. (2017). Modelling large plastic deformations of cohesive soils using sequential limit-analysis, *Int. J. Numer. Anal. Meth. Geomech.*, **41**, 1781-1806.

Lacroix R., Leblond J.B. and Perrin G. (2016). Numerical study and theoretical modelling of void growth in porous ductile materials subjected to cyclic loadings, *Eur. J. Mech. - A/Solids*, **55**, 100-109.

Lahellec N. and Suquet P. (2007). On the effective behavior of nonlinear inelastic composites: I. Incremental variational principles, *J. Mech. Phys. Solids*, **55** 1932–1963.

Leblond J.B., Kondo D., Morin L. and Remmal A. (2018). Classical and sequential limit-analysis revisited, *Comptes Rendus Mécanique*, bf 346, 336–349.

Leblond J.B. and Morin L. (2014). Gurson's criterion and its derivation revisited, *ASME J. Appl. Mech.*, **81**, 051012-1 to 7.

Leblond J.B., Perrin G. and Devaux J. (1995). An improved Gurson-type model for hardenable ductile metals, *Eur. J. Mech. A/Solids*, **14**, 499-527.

Leu S.Y. (2007). Analytical and numerical investigation of strain-hardening viscoplastic thick-walled cylinders under internal pressure by using sequential limit analysis, *Comput. Meth. Appl. Mech. Engng.*, **196**, 2713-2722.

Leu S.Y. and Li R.S. (2012). Exact solutions of sequential limit-analysis of pressurized cylinders with combined hardening based on a generalized Holder inequality: Formulation and validation, *Int. J. Mech. Sc.*, **64**, 47-53.

Madou K., Leblond J.B. (2012a). A Gurson-type criterion for porous ductile solids containing arbitrary ellipsoidal voids - I: Limit-analysis of some representative cell. *J. Mech. Phys. Solids*, **60**, 1020-1036.

Madou K., Leblond J.B. (2012b). A Gurson-type criterion for porous ductile solids containing arbitrary ellipsoidal voids - II: Determination of yield criterion parameters. *J. Mech. Phys. Solids*, **60**, 1037-1058.

Madou K., Leblond J.B. (2013). Numerical studies of porous ductile materials containing arbitrary ellipsoidal voids - I: Yield surfaces of representative cells. *Eur. J. Mech. A/Solids*, **42**, 480-489.

Madou K., Leblond J.B., Morin L. (2013). Numerical studies of porous ductile materials containing arbitrary ellipsoidal voids - II: Evolution of the length and orientation of the void axes. *Eur. J. Mech. A/Solids*, **42**, 490-507.

Mandel J. (1964). Contribution théorique à l'étude de l'écrouissage et des lois d'écoulement plastique, in: *Proceedings of the 11th International Congress on Applied Mechanics*, Munich, FRG, Springer, pp. 502-509 (in French).

Mbiakop A., Constantinescu A. and Danas K. (2015). On void shape effects of periodic elasto-plastic materials subjected to cyclic loading, *Eur. J. Mech. A/Solids*, **49**, 481-499.

Mear M. and Hutchinson J. (1985). Influence of yield surface curvature on flow localization in dilatant plasticity, *Mech. Mater.*, **4**, 395-407.

Morin L., Michel J.C. and Leblond J.B. (2017). A Gurson-type layer model for ductile porous solids with isotropic and kinematic hardening, *Int. J. Solids Structures*, **118-119**, 167-178.

Nielsen K.L., Andersen R.G. and Tvergaard V. (2018). Void coalescence mechanism for combined tension and large amplitude cyclic shearing, *Engng. Fract. Mech.*, **189**, 164–174.

Rabold F. and Kuna M. (2005). Cell model simulation of void growth in nodular cast iron under cyclic loading, *Comput. Mater. Sci.*, **32**, 489-497.

Remmal A. (2021). Extension de l'approche locale de la rupture ductile aux sollicitations cycliques de grandes amplitudes, Ph.D. Thesis, Sorbonne Université, Paris.

Schmidt R.A., Wilkowski G.M. and Mayfield M.E. (1991). The International Piping Research Group (IPIRG) program. An overview, *11th International Conference on Structural Mechanics in Reactor Technology (SMIRT 11)*, Tokyo, Japan, paper G23/1.

Steglich D., Pirondi A., Bonora N. and Brocks W. (2005). Micromechanical modelling of cyclic plasticity incorporating damage, *Int. J. Solids Structures*, **42**, 337-351.

Stolz C. (1987). Anélasticité et stabilité, Thèse d'Etat, Université Pierre et Marie Curie, Paris.

Tvergaard V. (1981). Influence of voids on shear band instabilities under plane strain conditions, *Int. J. Fracture*, **17**, 389-407.

Tvergaard V. and Needleman A. (1984). Analysis of the cup-cone fracture in a round tensile bar, *Acta Metall.*, **32**, 157-169.

Yang W.H. (1993). Large deformation of structures by sequential limit analysis, *Int. J. Solids Structures*, **30**, 1001-1013.

Yuan X.P., Maillot B. and Leroy Y.M. (2017). Deformation pattern during normal faulting: A sequential limit-analysis, *J. Geophys. Res. Solid Earth*, **122**, 1496-1516.

A Appendix : A simplified version of Chaboche (1991)'s cyclic plasticity model

The simple hardening rule (3) predicts a "saturation" of the yield limit $\overline{\sigma}$ for large plastic strains, once the ultimate stress is reached. Therefore, under cyclic loadings with fixed strain amplitude, once both the isotropic and kinematic hardening variables have reached their stationary values, the cyclic stress-strain curve stabilizes; and the stress amplitude of the stabilized curve, depending only on the saturated value of $\overline{\sigma}$, is independent of the strain amplitude.

However this prediction is incorrect in practice: it is well-known experimentally that in stainless steels for instance, the stabilized cyclic curve depends on the previous mechanical history. To fix this problem, Chaboche (1991) proposed to make $\overline{\sigma}$ a function of the "maximum strain amplitude" q of the previous cycles. To measure this "amplitude", he introduced a 6-dimensional strain domain within the space of strain tensors, spanned in time by the actual plastic strain tensor, analogous to the reversibility domain in the space of stress tensors. The radius of this strain domain defined the amplitude q.

Chaboche (1991)'s model is complex and numerically cumbersome, because of the 6D nature of the strain domain. We therefore use here a simplified variant of this model, sufficient for most practical purposes, wherein Chaboche (1991)'s 6D strain domain is replaced by a mere segment on the real line. The original and simplified versions of the model yield strictly identical predictions for proportional strain loadings (that is, for which $\mathbf{d}^p$ retains a constant direction in the strain space). To define the 1D strain domain, we introduce the quantities

$$\overline{\epsilon}(t) \equiv \int_0^t \mathrm{sgn}[\mathrm{tr}\,\mathbf{d}(\tau)] d^p_{eq}(\tau) d\tau \quad , \quad \begin{cases} \overline{\epsilon}_{\max}(t) \equiv \max_{0\leq\tau\leq t} \overline{\epsilon}(\tau) \\ \overline{\epsilon}_{\min}(t) \equiv \min_{0\leq\tau\leq t} \overline{\epsilon}(\tau) \end{cases} \quad , \quad q \equiv \frac{1}{2}\left(\overline{\epsilon}_{\max} - \overline{\epsilon}_{\min}\right). \tag{A.1}$$

The quantity $\overline{\epsilon}$ is a kind of "algebraic cumulated plastic strain", which increases in "tension" ($\mathrm{tr}\,\mathbf{d} > 0$) but decreases in "compression" ($\mathrm{tr}\,\mathbf{d} < 0$); $\overline{\epsilon}_{\max}(t)$ and $\overline{\epsilon}_{\min}(t)$ are the maximum and minimum values of $\overline{\epsilon}$ reached until time t, so that $[\overline{\epsilon}_{\min}(t), \overline{\epsilon}_{\max}(t)]$ is the interval spanned by $\overline{\epsilon}$ during the previous mechanical history; and q is the "radius" (half-length) of this interval.

The yield limit $\overline{\sigma}$ is then defined by Chaboche (1991)'s evolution equation:

$$\frac{d\overline{\sigma}}{dt} = B\left[Q(q) - \overline{\sigma}\right]\frac{dp}{dt} \tag{A.2}$$

with the initial value $\overline{\sigma}(t=0) = \sigma_0$ where σ_0 is the initial yield stress (in the absence of hardening). In equation (A.2) B is a positive dimensionless constant which governs the evolution of $\overline{\sigma}$ toward its asymptotic value (at fixed q) $Q(q)$; and the function $Q(q)$ itself represents the set of "maximum points" of the stabilized cyclic curves, for gradually increasing strain amplitudes q (with, conventionally, $Q(q=0) = \sigma_0$).